Model Predictive Control-based 3D Navigation of a RIS-Equipped UAV for LoS Wireless Communication with a Ground Intelligent Vehicle

Mohsen Eskandari, Hailong Huang, Andrey V. Savkin, Wei Ni

***Abstract*[1]—Intelligent vehicles need high bandwidth wireless communication links for safety and commercial communication. However, the new generations of wireless communication networks (WCNs), such as quasi-optic millimeter-wave (mmWave) (5G) and visible light optic (6G) WCNs, are exposed to blockage/scattering problems in highly dense (urban) areas. In this paper, we propose a reconfigurable intelligent surface (RIS)-equipped (unmanned aerial vehicle) UAV (RISeUAV) to secure an uninterrupted line-of-sight (LoS) communication link for an intelligent vehicle. The vehicle can be a smart ambulance and needs a stable high-speed link for autonomous navigation, also for continuous monitoring/diagnosing of the health condition of a patient. A two-stage method is proposed to address the NP-hardness and nonconvexity of planning an optimal trajectory for autonomous navigation of the RISeUAV limited to UAV motion and LoS constraints. In the first stage, the optimal tube path is determined by considering the energy consumption, LoS link, and UAV speed/acceleration constraints. In the second stage, an accurate RISeUAV trajectory is obtained through the secured tube path by considering the communication performance, passive beamforming, and nonholonomic constraint of the RISeUAV. Dynamic programming and successive convex approximation methods are used in the first and second stages, respectively. Simulation results show the accuracy/effectiveness of the method.**

***Index Terms*—Autonomous navigation, optimal trajectory, reconfigurable intelligent surfaces (RISs), intelligent vehicles, unmanned aerial vehicles (UAVs), wireless communication.**

I. Introduction

Unmanned aerial vehicles (UAVs) are exploited in various civilian applications like parcel delivery, rescue operation, traffic monitoring [1], surveillance and data collection [2], assets maintenance, etc. Task appointment and target allocation to a single UAV or multiple UAVs and consequently path planning have been the main research topic [3]. Also, the autonomy of UAVs flight for completing the assigned tasks with minimum energy consumption and computational burden while achieving a satisfactory level of performance has been studied [4], [5].

As a key application, UAVs have been used to improve the performance of wireless communication networks (WCNs) [6]. In UAV-assisted WCNs, a UAV may act as an aerial active base station (BS) or aerial relay [7] to provide a direct link for user equipment. Also, UAVs can be used for data collection of widely distributed Internet-of-things (IoT) devices [8]. Optimal allocation [9], joint trajectory-power optimization [10], and positioning [11] are among the issues that have attracted extensive attention.

UAVs can support wireless communication for autonomous driving of intelligent vehicles in future smart cities thanks to their excellent 3D mobility. However, the overall loss of the quasi-optical millimeter-wave (mmWave) communication in the fifth-generation (5G) WCNs is significantly higher than that of microwave networks for a point-to-point link due to shadowing and blockage [12]. Also, beyond the 5G, sixth-generation (6G) optical communications require unobstructed links.

In the communication research community, efforts have been focused on solving problems with mmWave communication using massive multi-input multi-output (MIMO) BSs to secure robust ubiquitous connectivity, which makes the WCNs complex and energy-deficient. Nevertheless, the emerging reconfigurable intelligent surface (RIS) has been developed to enhance the spectral efficiency and spatial throughput of 5G WCNs exposed to path loss, coverage holes, and blockages [13]. RISs comprise reflective arrays or sub-wavelength metamaterial unit cells [14] that can be locally controlled to alter the amplitude and phase (shift) of the incident electromagnetic signal in a real-time reconfigurable manner [15]. The RIS can be mounted on the wall of buildings and using their intelligent reconfigurability, can produce favorable channel conditions for users by reflecting and beamforming the transmitted signal at the receiver side [16]. Further, the RIS does not have to possess signal processing capability which makes it energy efficient [17].

Enhanced UAV communication supported by stationary RISs also has gained attention in recent research works [18]. RISs are deployed to address the path loss issues of the UAV-assisted communication in the mmWave WCNs [19]. Along with the trajectory design and power minimization of UAVs [10], which are the concern of UAVs due to the limited onboard energy [20], the passive phase shift of RIS elements is an additive objective [21], which has been tackled in recent works [22], [23]. Lately, the RIS-equipped UAV (RISeUAV) technology has been considered in a few works for enhancing the flexibility and onboard energy efficiency of the next-generation WCNs [24], by reflecting in the sky and establishing clear/instant LoS links [25].

In this paper, we propose employ the RISeUAV to support LoS wireless communication for an intelligent vehicle in dense urban areas. The RISeUAV is used because the passive RIS avoids the complexity of the flying package and preserves the onboard energy. Besides, UAV communication (as an aerial active BS/relay in 5G-6G WCNs) might not be efficient in an obstructed environment, so the RISeUAV is a promising option with the aid of terrestrial cellular networks [26]. The intelligent vehicle can be an unmanned smart ambulance carrying a patient that needs a stable high bandwidth communication link for autonomous driving and continuously/remotely monitoring the patient's health conditions.

The real-time monitoring of patients involves the transmission of various clinical multimedia data, including videos, medical images, and vital signs, which requires the use of mobile networks with high-fidelity communication bandwidth [27].

[1] This work received funding from the Australian Government, via grant AUSMURIB000001 associated with ONR MURI grant N00014-19-1-2571.

However, quasi-optic mmWave communication might be interrupted when the vehicle moves through an obstructed dense urban area. With the aid of the RISeUAV, it is possible to ensure critical emergency services in a moving smart ambulance [28]. This target is achievable since the reliability of RIS-aided communication has been analyzed [13] and validated through experimental tests by successfully modulating/transmitting a digital video file through an RIS-based transmitter [29]. The application of RISeUAV is not limited to health/safety issues and can also be utilized in other applications, e.g., maintaining a secure and robust LoS link for security/police vehicles in 5G and beyond in optical/visible light WCNs.

The RISeUAV navigation should be designed as the optimal energy-efficient trajectory to successfully provide aerial LoS service for the mobile target (MT) (i.e., the intelligent vehicle). However, the modeling and formulation of the problem for maintaining the LoS link, while the RISeUAV trajectory is constrained by the MT movement, is a nontrivial task and has not been addressed in the literature. The problem statement and shortcomings of the existing literature are discussed as follows.

1) The RISeUAV should fly at a relatively low altitude to preserve the quality of the LoS communication links. Therefore, the RISeUAV may fly through buildings in dense urban areas. This constructs a problem of a 3D crash avoidance trajectory planning by considering the UAV motion constraints while following the MT. However, in most UAV-assisted communications, 2D unobstructed path planning has been considered for static or quasi-static targets [20]-[23]. For example, the problem of finding the optimum trajectory of a rotary-wing UAV, as an aerial BS to communicate with some stationary ground nodes, was formulated as convex programming [20]. However, the problem is solved after some simplifications, e.g., at a fixed attitude through an unobstructed path and at a constant speed.
2) For autonomous navigation, the optimal trajectory should be designed in real time by the RISeUAV's overhead controller [30]. This makes the problem computationally challenging since it is time-consuming to validate the 3D state-space for finding the optimal collision-free path that satisfies the problem constraints [31]. Besides, the valid state-space dynamically changes and is time-varying in nature due to the MT movement through the buildings, making the optimization problem non-convex. Real-time obstacle detection has been studied [32]. However, optimal path planning in a dynamic environment is an open research topic.
3) The most critical problem is formulating the LoS service into an optimization problem. To the best of our knowledge, no work in the relevant literature has elaborated on this issue. Considering the energy-efficient path and channel performance as the objectives, maintaining valid LoS links can be modeled in the optimization as a constraint. In this light, spots, where RISeUAV does not provide an LoS link for the MT, can be regarded as fictitious obstacles that must be avoided. However, modeling these dynamic fictitious obstacles as the constraints is NP-hard and nonconvex.
4) After validating the state space, the problem of finding the optimal solution, i.e., energy-efficient trajectory, can be reduced to the NP-hard traveling salesman problem (TSP) with neighborhood. Also, the communication channel performance and RIS phase shift for beamforming impose additional objectives/constraints.

Therefore, we deal with a multilateral problem with the non-convex optimization and its convergence to a valid solution while considering the computational burden. To address these issues, the contributions of the paper are listed as follows.

- This paper, for the first time, studies the application of a RISeUAV to establish an uninterruptable LoS wireless communication link for an intelligent vehicle. The navigation is modeled as a real-time optimization problem to design the trajectory that satisfies problem constraints.
- To tackle the computational hardness of the problem, a two-stage navigation scheme is proposed by utilizing the receding finite horizon model predictive control (MPC) and dynamic programming (DP).
- In the first stage, energy consumption, LoS link, and navigation issues are considered using a semi-rapidly exploring tree (RRT) method. The optimal energy-efficient tube path is planned based on the map route of the MT, maneuver limits associated with the UAV (speed/acceleration constraints), and the environment 3D plan with potential blockage/obstacles to secure the LoS. The tube path provides a permitted cylindrical space for the UAV flight through which the UAV motion and LoS constraints are satisfied.
- In the second stage, an accurate UAV trajectory is obtained through the tube path considering the RIS phase shift and communication channel performance associated with the BS−RIS−MT link. The problem is formulated and solved using successive convex approximation.
- To obtain the exact optimal UAV trajectory, maximizing the achievable rate by maximizing the channel gain is considered through channel estimation and RIS reconfiguration. Further, the RIS position is not fixed in our application, which demands appropriate mathematical modeling for channel estimation that is delineated and developed in this paper.

The remainder of this paper is organized as follows. In Section II, the problem modeling and formulation are developed and the problem statement for UAV navigation is elaborated. In Section III, the proposed method for optimizing the 3D trajectory of the RISeUAV is presented. Computer simulations are conducted in Section IV to evaluate the performance of the proposed method. Finally, Section V concludes the paper.

Notice that, in terms of the mathematic notation in the paper, variable t indicates a continuous function of time, τ denotes a specific time instant, and k indicates a sampling time (timestep).

II. Problem Formulation and Statement

A. UAV Motion and Energy Consumption Model

Let us model the position and heading of the RISeUAV by

$$p(\tau)\measuredangle\theta(\tau) \coloneqq [x(\tau),\ \ y(\tau),\ \ z(\tau)]^T\measuredangle\theta(\tau), \tag{1}$$

where $p(\tau) \in \mathbb{R}^{1\times 3}$ denotes the RISeUAV position in the Cartesian coordinates at time τ; $\theta(\tau)$ is the heading (yaw angle) of the RISeUAV with respect to the x −axis, and superscript T denotes matrix transpose. The UAV agility is of concern in the RISeUAV navigation for this application. Thus, we model the RISeUAV motion by the following kinematic equation of motion [33]:

$$\begin{aligned}
&\dot{x}(t) = v_x(t) = v(t)\cos\big(\theta(t)\big);\\
&\dot{y}(t) = v_y(t) = v(t)\sin\big(\theta(t)\big);\\
&\dot{z}(t) = u(t) - u_0;\\
&\dot{\theta}(t) = \omega(t);
\end{aligned} \tag{2}$$

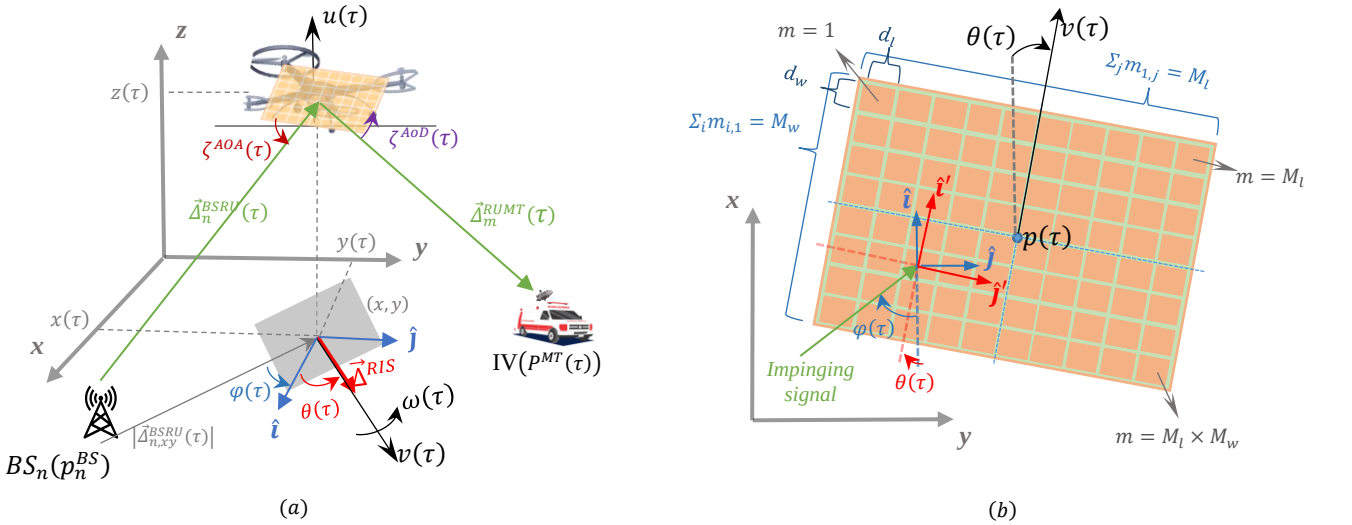

Fig. 1. The RISoUAV position and motion in the Cartesian coordinates: (a) 3D frame of the occupancy map (as the reference frame); (b) the yx−plane. Notice that the coordinates of the reference frame is converted to the RIS-frame using transformation matrix $\Gamma(\theta(\tau))$.

where $v(t) = \left\| [v_x(t), v_y(t)]^T \right\|_2$, $u(t)$, and $\omega(t)$ are linear horizontal, vertical and angular speeds, respectively; $\|\cdot\|$ is norm operator, and u_0 denotes the base vertical speed input for hovering. The roll and pitch (elevation) angles are assumed to be fixed in this paper. The roll and pitch (elevation) angles can also be considered optimization variables and can be considered in future works.

Consider $U(t) = [v_x(t)\ v_y(t)\ u(t)\ \omega(t)]^T$ as the input to the RISeUAV motion model in (2). The following energy cost function can be considered for the RISeUAV navigation:

$$E_{RISoUAV} = \int_{t_0}^{t_0+\mathcal{T}} \Big(\alpha_1 \left\| v_x(t), v_y(t) \right\|_2 + \alpha_2 |u(t)| + \alpha_3 |\omega(t)| + \alpha_4 \left\| \dot{v}_x(t), \dot{v}_y(t) \right\|_2 + \alpha_5 |\dot{u}(t)| + \alpha_5 |\dot{\omega}(t)| \Big) dt, \quad (3)$$

where $E_{RISoUAV}$ denotes the energy consumption of the UAV, $\mathcal{T}$ denotes the time interval of interest in the $[t_0, \ t_0 + \mathcal{T}]$ interval; $\alpha_1 > 0$, $\alpha_2 > 0$, $\alpha_3 > 0$, $\alpha_4 > 0$, $\alpha_5 > 0$, and $\alpha_6 > 0$ are weighting coefficients that compromise the control inputs and UAV maneuver (hovering and propulsion/acceleration).

B. State-Space, Occupancy Map, and LoS Model

The urban area can be mapped onto a 3D occupancy map using a Lidar sensor [34], and the 3D map is uploaded to the RISeUAV's onboard controller. Fig. 1(a) shows the RISeUAV position and motion in the Cartesian coordinate system. We assume that the RIS is symmetrically mounted to the balanced center of the UAV (to preserve flight stability) facing the ground. Therefore, $p(\tau)$ denotes the center point of the RIS and the coordinates of the RIS elements (unit cells or reflectarrays) can be calculated by the UAV coordinates and dimensions of elements. The 3D frame of the occupancy map is considered the reference frame. $\Gamma(\theta(\tau)) \in \mathbb{R}^{3\times3}$ converts the coordinates from the reference frame to the RIS frame (with the shifted angle $\theta(\tau)$ given by the UAV heading at time τ):

$$\Gamma(\theta(\tau)) = \begin{bmatrix} \cos(\theta(\tau)) & -\sin(\theta(\tau)) & 0 \\ \sin(\theta(\tau)) & \cos(\theta(\tau)) & 0 \\ 0 & 0 & 1 \end{bmatrix}.$$

Let $p_m(\tau) = [x_m(\tau), \ y_m(\tau), \ z_m(\tau)]^T \in \mathbb{R}^{1\times3}$ denote the coordinates of the m^{th} element of the RIS at time τ, where $m \in \mathcal{M} = \{1, \dots, M\}$ and M is the number of RIS elements. Therefore, the coordinates of element m are obtained as:

$$p_m(\tau) = \Gamma^{-1}(\theta(\tau)) \left(\begin{bmatrix} x(\tau) \\ y(\tau) \\ z(\tau) \end{bmatrix} + \begin{bmatrix} w(m) \\ l(m) \\ 0 \end{bmatrix} \right), \quad (4)$$

where

$$w(m) = d_w \left(\left(\frac{M_w + 1}{2} \right) - \left\lceil \frac{m}{M_l} \right\rceil \right);$$

$$l(m) = d_l \left(Mod(m-1, M_l) - \left(\frac{M_l - 1}{2} \right) \right);$$

M_l and M_w are the number of elements along with the length and width of the RIS, respectively; and d_l and d_w denote the length and width sizes of the elements respectively, see Fig. 1(b). Here $\lceil \cdot \rceil$ and $Mod(.,.)$ are the round-up and modulus functions, respectively.

Let $p_n^{BS} = [x_n^{BS}, \ y_n^{BS}, \ z_n^{BS}]^T \in \mathbb{R}^{1\times3}$ denote the coordinates of the n^{th} BSs, where $n \in \mathcal{N} = \{1, \dots, N\}$ and N is the number of BSs installed in the geographical area of interest, and $p^{MT}(\tau) = [x^{MT}(\tau), \ y^{MT}(\tau), \ 0]^T \in \mathbb{R}^{1\times3}$ denote the MT (vehicle) position at time τ. Accordingly, we have $\vec{\Delta}_{nm}^{BSRU}(\tau) = p_m(\tau) - p_n^{BS}$, $\vec{\Delta}_m^{RUMT}(\tau) = P^{MT}(\tau) - p_m(\tau)$, and $\vec{\Delta}_n^{BSMT}(\tau) = P^{MT}(\tau) - p_n^{BS}$ denoting the vector from the n^{th} BS to the m^{th} elements of the RIS (i.e., the BS−RISeUAV link), the vector from the m^{th} element of the RIS to the MT (i.e., the RISeUAV−MT link), and the vector from the n^{th} BS to the MT (i.e., the BS−MT link), respectively. For example:

$$\vec{\Delta}_{nm}^{BSRU}(\tau) = [x_m(\tau) - x_n^{BS}, \ y_m(\tau) - y_n^{BS}, \ z_m(\tau) - z_n^{BS}]^T.$$

The vector lengths, i.e., $|\vec{\Delta}_{nm}^{BSRU}(\tau)|$, $|\vec{\Delta}_m^{RUMT}(\tau)|$, and $|\vec{\Delta}_n^{BSMT}(\tau)|$, denote the BS−RISeUAV, RISeUAV−IV, and BS−MT Euclidean distances (norms), respectively. For instance:

$$|\vec{\Delta}_{nm}^{BSRU}(\tau)| = \left\| \vec{\Delta}_{nm}^{BSRU}(\tau) \right\|_2 = \sqrt{(x_m(\tau) - x_n^{BS})^2 + (y_m(\tau) - y_n^{BS})^2 + (z_m(\tau) - z_n^{BS})^2}.$$

Alternatively, $\vec{\Delta}_{nm}^{BSRU}(\tau) = (x_m(\tau) - x_n^{BS})\hat{\mathbf{i}} + (y_m(\tau) - y_n^{BS})\hat{\mathbf{j}} + (z_m(\tau) - z_n^{BS})\hat{\mathbf{k}}$, where $\hat{\mathbf{i}}$, $\hat{\mathbf{j}}$, and $\hat{\mathbf{k}}$ are the vectors of the unit length along the $x, y,$ and z axes, respectively. The normalized vector of the RISeUAV (on the xy−plane) is given as: $\vec{\Delta}^{RU} = \cos(\theta(\tau))\,\hat{\mathbf{i}} + \sin(\theta(\tau))\,\hat{\mathbf{j}}$, where $\theta(\tau)$ is the heading (yaw) angle at time τ. Subscript "xy" indicates the 2D Euclidean distance on

the xy−plane.

Suppose that $\Omega \in \mathbb{R}^3$ is a set of coordinates that belong to the 3D map of the dense urban area. Let $p_\Omega^{3D} = \{[x_{ij}^{3D} \ y_{ij}^{3D} \ z_{ij}^{3D}] | \forall\, i \in \{1, \dots, \mathcal{P}_j\}, j \in \{1, \dots, \Im\} \in \Omega\}$, where $\mathcal{P}_j$ denotes the number of the Cartesian coordinates of the j^{th} building and $\Im$ is the number of buildings. The LoS components for vectors $\vec{\Delta}_{nm}^{BSRU}(\tau)$, $\vec{\Delta}_{m}^{RUMT}(\tau)$ and $\vec{\Delta}_{n}^{BSMT}(\tau)$ are modeled as:

$$\mathrm{LoS}_{nm}^{BSRU}, \mathrm{LoS}_{m}^{RUMT}, \mathrm{LoS}_{n}^{BSMT} = \begin{cases} 1, & if\ \vec{\Delta}_{nm}^{BSRU}(\tau), \vec{\Delta}_{m}^{RUMT}, \vec{\Delta}_{n}^{BSMT} \cap\ p_\Omega^{3D} = \emptyset \\ 0, & if\ \vec{\Delta}_{nm}^{BSRU}(\tau), \vec{\Delta}_{m}^{RUMT}, \vec{\Delta}_{n}^{BSMT} \cap\ p_\Omega^{3D} \neq \emptyset \end{cases} \quad (5)$$

which are treated as the LoS constraints in the RISeUAV navigation problem. The validity of the LoS link can be tested by interpolating the corresponding vector and checking the membership of intermediate points with the occupancy map.

C. Channel Model

The RIS comprises a uniform linear array of reflective elements as a specular reflector [14], and the phase shift of each element is controlled via an embedded controller at the UAV. The phase-shift matrix of the RIS is $\Theta(\tau) = \mathrm{diag}\{e^{j\vartheta_1(\tau)}, e^{j\vartheta_2(\tau)}, \dots, e^{j\vartheta_M(\tau)}\}$, where diag(.) denotes a diagonal matrix and $\vartheta_i(\tau) \in [0, 2\pi), i \in \mathcal{M}$ is the phase-shift of the i^{th} RIS element at time τ. Here, it is worth noting that since the RISeUAV chases a fast-moving vehicle, the compatibility of the response time of the RIS controller with RISeUAV motion, i.e., limitations on continuous phase shift, must be considered in the optimization of the trajectory and speed which can be considered in future works. The impact of channel state information (CSI) imperfection on RIS-assisted communication has been studied in the literature, e.g., [35], and is not elaborated on in this paper.

Regarding the BS−MT link, since the LoS link can be randomly blocked by buildings and foliage, the Rayleigh channel fading model is utilized. The BS−MT channel gain is given by:

$$g_{BSMT}(\tau) = \left(\sqrt{\rho \left|\vec{\Delta}_n^{BSMT}(\tau)\right|^{-\gamma}}\right)\tilde{g}, \quad (6)$$

where ρ is the path loss at the reference distance (1 m), $\gamma \geq 2$ is the path loss exponent, and $\tilde{g}$ is a random scattering component modeled by a zero-mean and unit-variance circularly symmetric complex Gaussian (CSCG) random variable.

Since the RISeUAV trajectory is designed to secure the LoS link, the free-space path loss channel model is assumed in the BS−RISeUAV and RISeUAV−MT links. The channel gains are modeled as [13], [15]:

$$g_{BSRU}(\tau) = \sqrt{\rho}\left[\frac{e^{-j\phi_{n(m=1)}^{BSRU}(\tau)}}{\sqrt{\left|\vec{\Delta}_{n(m=1)}^{BSRU}(\tau)\right|^{\gamma}}}, \dots, \frac{e^{-j\phi_{nm}^{BSRU}(\tau)}}{\sqrt{\left|\vec{\Delta}_{nm}^{BSRU}(\tau)\right|^{\gamma}}}, \dots, \frac{e^{-j\phi_{nM}^{BSRU}(\tau)}}{\sqrt{\left|\vec{\Delta}_{nM}^{BSRU}(\tau)\right|^{\gamma}}}\right]^T, \quad (7)$$

where $\phi_{nm}^{BSRU}\left(\zeta_m^{AoA}(\tau), \varphi_m^{AoA}(\tau)\right)$ reflects the phase delay (shift) of the impinging signal from the BS to the m^{th} element of the RIS, and $\varphi_m^{AoA}(\tau)$ and $\zeta_m^{AoA}(\tau)$ are the azimuth and elevation angle-of-arrival (AoA) of the signal at time τ, respectively. Similarly, the channel gain of the RISeUAV−MT link is given by:

$$g_{RUMT}(\tau) = \sqrt{\rho}\left[\frac{e^{-j\phi_{RUMT}^{(m=1)}(\tau)}}{\sqrt{\left|\vec{\Delta}_{(m=1)}^{RUMT}(\tau)\right|^{\gamma}}}, \dots, \frac{e^{-j\phi_{RUMT}^{m}(\tau)}}{\sqrt{\left|\vec{\Delta}_{m}^{RUMT}(\tau)\right|^{\gamma}}}, \dots, \frac{e^{-j\phi_{RUMT}^{M}(\tau)}}{\sqrt{\left|\vec{\Delta}_{M}^{RUMT}(\tau)\right|^{\gamma}}}\right]^T, \quad (8)$$

where $\phi_{RUMT}^{m}\left(\zeta_m^{AoD}(\tau), \varphi_m^{AoD}(\tau)\right)$ reflects the phase delay (shift) of the incident signal from the m^{th} element of the RIS to the MT, and $\varphi_m^{AoD}(\tau)$ and $\zeta_m^{AoD}(\tau)$ are the azimuth and elevation angle-of-departure (AoD) of the incident signal at time τ, respectively.

The signal-to-noise ratio (SNR) at the MT through the BS−RISeUAV −MT and direct BS-MT links is obtained as:

$$\Upsilon_{BS-RU-MT}(\tau) = \frac{P_{BS}(\tau)\left|g_{BSMT}(\tau) + g_{RUMT}^H(\tau)\Theta(\tau)g_{BSRU}(\tau)\right|^2}{\sigma^2}, \quad (9)$$

where $\Upsilon_{BS-RU-MT}(\tau)$ is the SNR at time τ, $P_{BS}(\tau)$ is the power transmitted by the BS at time τ, and σ^2 is the noise power at MT. Finally, the achievable rate at the MT is obtained as:

$$R_{BS-RU-MT}(\tau) = \log_2\left(1 + \Upsilon_{BS-RU-MT}(\tau)\right). \quad (10)$$

D. Problem Formulation

We aim to achieve three objectives for the RISeUAV navigation:

1) Minimizing the energy consumption of the UAV: This also ensures the shortest path is selected for the RISeUAV, which helps to avoid violating the speed/acceleration limits by the UAV because the RISeUAV must follow the MT in time, which may move fast.

$$\min_{v_x(t), v_y(t), u(t), \omega(t)} E_{RISoUAV} \quad (11)$$

$$s.t. \quad \begin{matrix} 0 \leq v(t) \leq V_{max} \\ -U_{max} \leq u(t) \leq U_{max} \\ -W_{max} \leq \omega(t) \leq W_{max} \\ Z_{min} \leq z(t) \leq Z_{max} \end{matrix} \quad (12)$$

$$\begin{cases} -\dot{V}_{max} \leq \dot{v}(t) \leq \dot{V}_{max} \\ -\dot{U}_{max} \leq \dot{u}(t) \leq \dot{U}_{max} \\ -\dot{W}_{max} \leq \dot{\omega}(t) \leq \dot{W}_{max} \end{cases} \quad (13)$$

$$p(\tau) \cap p_\Omega^{3D} = \emptyset,\ \forall\, \tau \in [t_0, \quad t_0 + \mathcal{T}], \quad (14)$$

where V_{max}, U_{max}, and W_{max} are positive constants indicating the maximum linear horizontal, vertical and angular speeds, respectively; and Z_{min} and Z_{max} denote the minimum and maximum limits of the RISeUAV altitude, respectively; $\dot{V}_{max}$, $\dot{U}_{max}$ and $\dot{W}_{max}$ denote the horizontal, vertical, and angular acceleration limits, respectively. Constraints (12) and (13) impose velocity/altitude and acceleration limits, respectively. Constraint (14) ensures collision avoidance.

2) Passive beamforming for rate maximization via the BS−RISeUAV −MT LoS link: Since $\Upsilon_{BS-RU-MT}(\tau) \geq 0$ and due to the concavity of the logarithmic function, we have $R_{BS-RU-MT}(\tau) \propto \Upsilon_{BS-RU-MT}(\tau)$, where $\propto$ denotes "proportional to". Also, the RISeUAV is a passive element in the WCN. In contrast to UAV-enabled communication [10], power control is out of concern. Besides, the RISeUAV provides an additive LoS link to the direct BS−MT channel, which is of interest in our study. Therefore, regarding the performance of the BS−RIS−MT LoS link, we consider the following objective function for optimizing the channel performance:

$$\max_{v(t),u(t),\omega(t),\Theta(t)} \Psi = \int_{t_0}^{t_0+\mathcal{T}} g_{RUMT}^{H}(\tau)\Theta(\tau)g_{BSRU}(\tau)\,d\tau, \quad (15)$$

$$s.t. \quad \Upsilon_{BS-RU-MT}(\tau) \geq SNR_{min}, \forall\, \tau \in [t_0, \quad t_0+\mathcal{T}], \quad (16)$$

$$(12), (13), (14),$$

where SNR_{min} denotes the minimum SNR. Constraint (16) ensures the minimum SNR is achieved at the MT through a direct BS−MT LoS link, otherwise through the RISeUAV and BS−RISeUAV −MT LoS link at each time. We can develop the channel performance Ψ as a function of the BS−RISeUAV −MT LoS link and phase shift matrix as given by

$$\Psi = \int_{t_0}^{t_0+\mathcal{T}} \rho \sum_{n=1}^{N}\sum_{m=1}^{M} \frac{e^{j\left(\vartheta_m(\tau)+\left(\phi_m^{RUMT}(\tau)-\phi_{nm}^{BSRU}(\tau)\right)\right)}}{\sqrt{\left(\left|\vec{\Delta}_m^{RUMT}(\tau)\right|\left|\vec{\Delta}_{nm}^{BSRU}(\tau)\right|\right)^{\gamma}}} d\tau; \quad (17)$$

It is evident from (17) that the performance of the BS−RISeUAV −MT channel depends on the phase shift matrix and is adversely affected by the length/distance of the BS−RIS−MT LoS link.

3) Securing uninterrupted BS−RIS−MT LoS link. We model this objective as the LoS constraint, applying to both objective functions (11) and (15), as

$$\exists(BS_n)|\left(\vec{\Delta}_n^{BSRU}(\tau) \cup \vec{\Delta}^{RUMT}(\tau)\right) \cap\ p_{\Omega}^{3D} = \emptyset; \quad (18)$$

III. The Proposed Solution for RISeUAV Navigation

The MT map route $\mathfrak{R}$, from the starting position of the MT to its destination, is known, as it can be yielded by maps Apps. The MT communicates the map route with the RISeUAV. The RISeUAV must hold the continuous (BS−RIS−IV) LoS link while satisfying the speed and SNR constraint through an energy-efficient path with optimal channel performance. However, the RISeUAV must follow the MT at a close distance to maintain the LoS link in an obstructed environment. This issue along with the RISeUAV motion constraints imposes some limitations on the RISeUAV trajectory design, making the navigation an NP-hard optimization problem.

A two-stage autonomous navigation model for RISeUAV is presented in this section by designing the optimal trajectory. Stable tracking control through the obtained trajectory [36] is beyond the scope of this paper. Here, the trajectory is a flight path in which RISeUAV flight speed/time is considered.

A. Stage 1. Energy-Efficient Obstacle-free Tube Path

At this stage, the RISeUAV's random possible paths are determined by utilizing a semi-RRT algorithm. Then, using the MPC method [33], prospective trajectories are achieved, which satisfy the problem constraints, i.e., speed/acceleration limits and LoS constraints. Then, dynamic programming is used to achieve the optimal trajectory with the minimum UAV energy consumption.

To MT route $\mathfrak{R}$ is divided into K waypoints with relatively large distances. The map route is modeled by $\mathfrak{R}: \{\mathfrak{R}[k]|\ \forall\, k \in \mathcal{K} = \{0, 1, \dots, K\}\}$ that includes the start, middle, and endpoints of streets (direct routes) in $\mathcal{K}$. Let $\mathcal{T}[k]$ be the time indicator (i.e., the time period) that the MT takes to move from $\mathfrak{R}[k-1]$ to $\mathfrak{R}[k]$ and is available based on the MT speed, so that $T = \sum_{k=1}^{K}\mathcal{T}[k]$, where T is the mission completion time determined by the MT. Therefore, the navigation model loses a degree of freedom and must obey the mission completion time enforced by the MT. This issue, along with the constraints associated with the LoS link and occupancy map of a dense area, heavily restrains the valid state space for RISeUAV navigation making the classic RRT computationally inefficient. Thus, we propose a modified RRT algorithm as described in the sequel.

For $\mathfrak{R}[k], \forall\, k \in \mathcal{K}$, some random options are assigned to the RISeUAV position as given by:

$$\mathcal{Q}[k, q_k] = Random\left(\left[p[k, q_k] \measuredangle \theta[k, q_k]\right]\right), \quad \forall\, k \in \mathcal{K}, \forall\, q_k \in \mathbb{Q}_k = \{1, \dots, Q_k\},$$

where $Random(.)$ denotes random of $(.)$; $[k, q_k]$ denotes the $q_k{}^{th}$ random option at the k^{th} waypoint, and Q_k is the number of random options for the k^{th} waypoint. We define $\mathcal{S}[k, q_k]$ as the sphere with $\mathcal{Q}[k, q_k]$ as being the center and the radius $\curlyvee$. Those of $\mathcal{Q}[k, q_k]$ for which the LoS and SNR prerequisites in (16) and (18) are not satisfied, and/or the associated sphere overlaps with the pre-specified spheres are omitted, and new random options that satisfy the constraints are replaced. Note that the altitude of random options must be higher than $z_n^{BS} + z$, where z is a positive value to ensure the LoS link is effective. Also, there should be a valid direct path between random options of waypoint $\mathfrak{R}[k]$ and allocated random options of waypoint $\mathfrak{R}[k-1]$. These constraints further limit the valid state space for RISeUAV path planning, which is against the computational time.

There are $\aleph$ number of prospective paths for RISeUAV along with $\mathfrak{R}(\mathfrak{R}[0]: \mathfrak{R}[K])$ comprising point-to-point (p2p) paths by considering all possible combinations of p2p paths:

$$\Xi_{1:\aleph}(\mathcal{Q}[0, q_0]: \mathcal{Q}[K, q_K]) = \{\Xi[1, q_0^1], \dots, \Xi[k, q_{k-1}^k], \dots, \Xi[K, q_{K-1}^K]\};$$

$$\Xi[k, q_{k-1}^k] = \Xi(\mathcal{Q}[k-1, q_{k-1}]: \mathcal{Q}[k, q_k]), \forall\, q_{k-1} \in \mathbb{Q}_{k-1}, \forall\, q_k \in \mathbb{Q}_k;$$

where $[k-1, q_{k-1}]$ denotes the $q_k{}^{th}$ random option at the $(k-1)^{th}$ waypoint. Totally $\aleph = Q^{K+1}$ is the number of prospective paths through the route $\mathfrak{R}$ from $\mathfrak{R}[0]$ to $\mathfrak{R}[K]$.

We yield the RISeUAV input (speed) associated with p2p prospective paths (corresponding to $\mathfrak{R}[k-1]$ to $\mathfrak{R}[k]$) starting from $\mathcal{Q}[k-1, q_{k-1}],\ \forall\, q_{k-1} \in \mathbb{Q}_{k-1}$, to $\mathcal{Q}[k, q_k], \forall\, q_k \in \mathbb{Q}_k$. The input speed corresponding to a given p2p path is defined as

$$U\left[k, q_{k-1}^k\right] = \left[v_x\left[k, q_{k-1}^k\right], v_y\left[k, q_{k-1}^k\right], u\left[k, q_{k-1}^k\right], \omega\left[k, q_{k-1}^k\right]\right],$$

where $U\left[k, q_{k-1}^k\right] = U(Q[k-1, q_{k-1}]: Q[k, q_k])$, which is obtained by plugging the coordinates of $\mathcal{Q}\left[k-1, q_{k-1}\right]$ and $\mathcal{Q}\left[k, q_k\right]$ into (19). Here, (19) is the discretized version of (2), as given by

$$U\left[k, q_{k-1}^k\right] = \frac{\mathcal{Q}\left[k, q_k\right] - \mathcal{Q}\left[k-1, q_{k-1}\right]}{\mathcal{T}[k]}, \quad (19)$$

The accelerations associated with the given p2p path are obtained as:

$$\dot{v}\left[k, q_{k-1}^k\right] = \left|\frac{v\left[k, q_{k-1}^k\right] - v\left[k-1, q_{k-2}^{k-1}\right]}{\mathcal{T}[k]}\right|$$

$$\dot{u}\left[k, q_{k-1}^k\right] = \left|\frac{u\left[k, q_{k-1}^k\right] - u\left[k-1, q_{k-2}^{k-1}\right]}{\mathcal{T}[k]}\right| \quad (20)$$

$$\dot{\omega}\left[k, q_{k-1}^k\right] = \left|\frac{\omega\left[k, q_{k-1}^k\right] - \omega\left[k-1, q_{k-2}^{k-1}\right]}{\mathcal{T}[k]}\right|$$

The speed and accelerations in (19) and (20) are obtained $\forall\ k \in \mathcal{K} - \{0\}, \forall\, q_{k-1} \in \mathbb{Q}_{k-1}, \forall\, q_k \in \mathbb{Q}_k$. The number of valid RRT branches is reduced because the corresponding branch of the tree (i.e., the p2p path) is discarded if the speed/acceleration constraints in (12) and (13) are not satisfied.

For each of the remaining branches (of each prospective

trajectory) the energy cost function is achieved using (21) which is obtained by discretizing (3):

$$E_{RISoUAV}^{\Xi_{\mathfrak{g}}} = \sum_{k\in\mathcal{K}-\{0\}} E_{RISoUAV}^{\Xi_{\mathfrak{g}}}[k, q_{k-1}^{k}]; \tag{21}$$

where

$$\begin{aligned} E_{RISoUAV}^{\Xi_{\mathfrak{g}}}[k, q_{k-1}^{k}] = {} & \alpha_1 \left(\left\| v_x[k, q_{k-1}^{k}], v_y[k, q_{k-1}^{k}] \right\|_2 \right) \\ & + \alpha_2 \left| u[k, q_{k-1}^{k}] \right| + \alpha_3 \left| \omega[k, q_{k-1}^{k}] \right| \\ & + \alpha_4 \left| \left\| \dot{v}_x[k, q_{k-1}^{k}], \dot{v}_y[k, q_{k-1}^{k}] \right\|_2 \right| \\ & + \alpha_5 \left| \dot{u}[k, q_{k-1}^{k}] \right| + \alpha_6 \left| \dot{\omega}[k, q_{k-1}^{k}] \right|, \end{aligned}$$

and $E_{RISoUAV}^{\Xi_{\mathfrak{g}}}$ denotes the energy consumption of the UAV through the $\mathfrak{g}^{th}$ prospective trajectory (Ξ_g). The trajectory with the minimum energy is adopted as the final trajectory:

$$\Xi^*(\, \mathcal{Q}[0, q_0]: \mathcal{Q}[K, q_K]\,) = \arg \min_{\substack{U[k,q_{k-1}^{k}]; \\ \forall k\in\mathcal{K}-\{0\}}} E_{RISoUAV}^{\Xi_{1:\aleph}} \tag{22}$$

Finally, the RISeUAV tube path Φ is achieved by connecting the spheres associated with the selected trajectory Ξ^*, as given by

$$\Phi^*(\, 0{:}\, K) = \{\mathcal{S}^*[0], \dots, (\mathcal{S}^*[k], U^*[k]), \dots, (\mathcal{S}^*[K], U^*[k])\}$$

where $U^*[k] \leftarrow U[k, {q^*}_{k-1}^{k}]$, $\mathcal{S}^*[k] \leftarrow \mathcal{S}[k, q_k^*]$, and q_k^* denotes the optimally selected random options at $\Re[k]$. However, browsing the most energy-efficient trajectory 1 is an NP-hard problem and can be formulated as Travelling Salesman Problem. In other words, the optimum trajectory cannot be found in polynomial time using an exhaustive search algorithm. Particularly, when the density of the urban area is high and/or the map route is long and the number of discretized waypoints and corresponding random options are large, finding the solution is time-consuming, with a time complexity of $O(Q^{K+1})$. To make the problem computationally tractable, we use dynamic programming.

Remark. Based on Bellman's principle [37], the optimum trajectory $\Xi^*(\, \mathcal{Q}[k, q_k]: \mathcal{Q}[K, q_K])$ satisfies the following Hamilton-Jacobi-Bellman (HJB) equation:

$$\begin{aligned} & \Xi^*(\, \mathcal{Q}[k, q_k]: \mathcal{Q}[K, q_K]) \\ & \quad = \min_{U[k,q_{k-1}^{k}]} \{\Xi[k, q_{k-1}^{k}] \\ & \quad + \Xi^*(\, \mathcal{Q}[k+1, q_{k+1}^*]: \mathcal{Q}[K, q_K^*])\}, \end{aligned} \tag{23}$$

which means starting from the last waypoint (i.e., the K^{th} waypoint) and selecting the p2p trajectory with the minimum energy consumption and keeping the process all the way to the starting point, the optimum trajectory is achieved. However, DP does not lead to the optimum solution because although the last p2p trajectory is optimal, it does not guarantee the optimality of the $(K-1)^{th}$ position as the endpoint of the next p2p trajectory.

To address this issue, we consider a weighting coefficient for random options, which is also aligned with the problem objectives, as follows. Based on (17), the distances between the RISeUAV and the BS, and between RISeUAV and MT adversely affect the channel performance. Therefore, we weigh each random option with its corresponding LoS link distance as given by

$$\begin{aligned} W(\, \mathcal{Q}[k, q_k]) = {} & (|\vec{\Delta}^{RUMT}(\mathcal{Q}[k, q_k])||\vec{\Delta}_n^{BSRU}(\mathcal{Q}[k, q_k])|); \\ & \forall\, q_k \in \mathbb{Q}_k, k \in \mathcal{K}. \end{aligned} \tag{24}$$

Then, we score each p2p trajectory with the following factor

$$\begin{aligned} F[k, q_{k-1}^{k}] = {} & E_{RISoUAV}[k, q_{k-1}^{k}] \\ & \times w_C \left(W(\, \mathcal{Q}[k-1, q_{k-1}]) \times W(\, \mathcal{Q}[k, q_k]) \right), \end{aligned} \tag{25}$$

where w_C is a positive coefficient to balance energy efficiency and channel performance. The smaller w_C the closer the solution to the energy-efficient trajectory. The index F is obtained by multiplication of the energy consumption index of the p2p trajectory to the product of the LoS link weights of its ends. Therefore, the p2p trajectory is selected to minimize (25), as given by

$$\Xi^*[k, q_{k-1}^{k}] = \arg \min_{U[k,q_{k-1}^{k}]} F[k, q_{k-1}^{k}]. \tag{26}$$

Then, DP finds the optimum solution based on (23), as explained in the following. The last p2p trajectory that minimizes $F[K, q_{K-1}^{K}]$ in (25), is selected. Then starting from the $\mathcal{Q}[K-1, q_{K-1}^*]$ associated with the selected p2p trajectory, in a recursive manner, the optimal p2p trajectory corresponding to the next (i.e., the $(K-1)^{th}$) discretized p2p path is selected. The process repeats until the first p2p trajectory is determined. At each p2p path where the trajectory is terminated due to the problem constraints (i.e., RISeUAV motion constraints), the next optimal p2p trajectory associated with the $(k+1)^{th}$ p2p path is selected. Finally, $\Phi^*(\, 0{:}\, K)$ is achieved. This technique significantly reduces the computational burden, because it does not explore and sort all valid trajectories for calculating corresponding energy consumption or scoring gain F. In the simulation section, we show that 90% optimality is achieved with less than 1% of the computational burden.

In stage 2, the exact RISeUAV trajectory is obtained through the tube path Φ^* by optimizing channel performance.

B. Stage 2. RISeUAV Trajectory and Passive Beamforming

After achieving the secure tube path, the channel performance is considered to obtain the optimal RISeUAV trajectory through the tube path. To this end, optimizing the objective function in (15), i.e., maximizing the BS−RIS−MT channel gain, is considered. However, the optimization problem in (15) is non-convex regarding the RISeUAV trajectory variables, i.e., $U(t)$, and phase-shift matrix of the RIS ($\Theta(t)$).

We solve the optimization problem in (15) by proposing tube-based finite receding horizon predictive control. The tube-based method limits possible solutions to predefined/valid boundaries, which helps to reduce the computational burden. In this regard, we discretize the tube path $\Phi^*[k]$ (i.e., the p2p trajectory $\Re[k-1]{:}\Re[k]$) into $\mathcal{E}$ slots as $\Phi^*[k, \epsilon]\ \forall\, \epsilon \in \mathbb{E} = \{1, \dots, \mathcal{E}\}$ where $\mathcal{E}$ is considered as the finite receding horizon for maximizing the achievable rate through the LoS channel for the upcoming p2p trajectory. Thus, (17) is updated for $\Phi^*[k]$ as:

$$\begin{aligned} & \Psi(p[k, \epsilon], \Theta[k, \epsilon], \forall\, \epsilon \in \mathbb{E}) \\ & = \rho \sum_{\epsilon=1}^{\mathcal{E}} \sum_{n=1}^{N} \sum_{m=1}^{M} \frac{e^{j\left(\vartheta_m[k,\epsilon] + \left(\phi_m^{RUMT}[k,\epsilon] - \phi_{nm}^{BSRU}[k,\epsilon]\right)\right)}}{\sqrt{\left(|\vec{\Delta}_m^{RUMT}[k, \epsilon]||\vec{\Delta}_{nm}^{BSRU}[k, \epsilon]|\right)^{\gamma}}} \\ & \quad p[k, \epsilon] \in \Phi^*[k, \epsilon], \vartheta_m[\epsilon] \in [0, 2\pi), \forall\, \epsilon \in \mathbb{E} \end{aligned} \tag{27}$$

where $p[k, \epsilon]$ denotes the RISeUAV position in (1) at the ϵ^{th} slot associated with the k^{th} p2p trajectory. The optimization problem is to find a set of positions $\{p[k, \epsilon] |\, \forall\, \epsilon \in \mathbb{E}\} \in \Phi^*[k]$ for the RISeUAV so that channel gain, and thus the achievable rate, are maximized through tube path $\Phi^*[k]$. To this end, we can regulate the phase-shift of the RIS elements, i.e., $\vartheta_m, \forall\, m \in \mathcal{M}$, to compensate for the phase delay associated with the BS−RIS−MT link. As a result, the associated received energy of all signals in the MT is accumulated coherently.

The phase delay associated with the incident signal from mobile BS to the m^{th} RIS element is obtained as

$$\phi_{nm}^{BSRU}[k,\epsilon] = \frac{2\pi}{\lambda}\mathbb{w}(\zeta_m^{AoA}[k,\epsilon],\varphi_m^{AoA}[k,\epsilon])\left(\vec{\Delta}_{nm}^{BSRU}[k,\epsilon]\right), \tag{28}$$

where λ is the carrier wavelength; and $\mathbb{w}(\zeta_m^{AoA},\varphi_m^{AoA}) \in \mathbb{R}^{1\times 3}$ is the planar wave vector as given by

$$\mathbb{w}(\zeta_{AoA}^m,\varphi_{AoA}^m) = \begin{bmatrix}\cos(\zeta_m^{AoA})\cos(\varphi_m^{AoA})\\ \cos(\zeta_m^{AoA})\sin(\varphi_m^{AoA})\\ \sin(\zeta_m^{AoA})\end{bmatrix}^T. \tag{29}$$

It is worth noting that the $\mathbb{w}(\zeta_m^{AoA},\varphi_m^{AoA}) \times \vec{\Delta}_{nm}^{BSRU}$ term in (28) results in the vector length $\left|\vec{\Delta}_{nm}^{BSRU}\right|$ (i.e., the Euclidean distance in the reference frame). Therefore, ϕ_{nm}^{BSRU} can be obtained as $(2\pi/\lambda) \times \left|\vec{\Delta}_{nm}^{BSRU}\right|$. Nevertheless, (28) can be used for the spatial scattering channel model used in the meta surface-based RIS, to obtain $\Gamma(\theta) \times \mathbb{w}\left(\zeta_m^{AoA},\varphi_m^{AoA}\right)$, i.e., the azimuth and elevation angle at the RIS frame, where optimizing the entire phase gradient is required for the optimal phase shift [14].

Similarly, the phase delay of the RIS-MT link for individual RIS elements (i.e., $\phi_m^{RUMT}(\zeta_m^{AoD},\varphi_m^{AoD})$) can be achieved. To compensate for the phase delay of the BS−RIS−MT link in (27) we consider:

$$\vartheta_m[k,\epsilon] = (\phi_{nm}^{BSRU}[k,\epsilon] - \phi_m^{RUMT}[k,\epsilon]) \qquad \forall\, \epsilon, m \tag{30}$$

Thus, (27) is updated as:

$$\Psi(p[k,\epsilon], \forall\, \epsilon \in \mathbb{E}) = \rho \sum_{\epsilon=1}^{\mathcal{E}}\sum_{n=1}^{N} \frac{M}{\sqrt{\left(\left|\vec{\Delta}^{RUMT}[k,\epsilon]\right|\left|\vec{\Delta}_n^{BSRU}[k,\epsilon]\right|\right)^{\gamma}}}; \tag{31}$$

$$p[k,\epsilon] \in \Phi^*[k], \forall\, \epsilon \in \mathbb{E}.$$

The problem is reduced to minimizing the denominator in (31) which is the sum of products of the BS−RISeUAV and RISeUAV−MT distances for all adjacent BSs. In scenarios where the MT moves in the inter-cell areas, the RISeUAV can be navigated to preserve its distance with adjacent BSs to improve the channel performance. However, this demands proper channel assignment and power control, which also complicates the phase shift algorithm. Alternatively, the BS associated with the cellular network covering the area corresponding to the p2p trajectory $[k]$, is taken. Note that the validity of the LoS link with the approaching BS (whose corresponding cell covers the next p2p trajectory), is guaranteed in the first stage. Therefore, the following objective function is considered:

$$\min_{U[k,\epsilon]} \quad \sum_{\epsilon=1}^{\mathcal{E}} \left|\vec{\Delta}^{RUMT}[k,\epsilon]\right|\left|\vec{\Delta}_n^{BSRU}[k,\epsilon]\right|, \tag{32}$$

$$s.t. \quad U_{max} \le U[k,\epsilon] \le U^*[k], \forall\, \epsilon \in \mathbb{E}, \tag{33}$$

$$p[k,\epsilon] \in \Phi^*[k], \forall\, \epsilon \in \mathbb{E}, \tag{34}$$

$$p[k,\mathcal{E}] \in \mathcal{S}^*[k], \tag{35}$$

$$\left(\vec{\Delta}_n^{BSRU}[k,\epsilon] \cup \vec{\Delta}^{RUMT}[k,\epsilon]\right) \cap\ p_\Omega^{3D} = \emptyset, \tag{36}$$

$$\Upsilon_{BS-RU-MT}[k,\epsilon] \ge SNR_{min}, \forall\, \epsilon \in \mathbb{E}, \tag{37}$$

where $U^*[k]$ is the optimal speed corresponding to p2p trajectory k achieved by stage one. Constraint (33) entails that the RISeUAV speed must be larger than the secured speed achieved at stage one for the k^{th} p2p trajectory, subject to the UAV maximum speed. Constraint (34) ensures that the RISeUAV flies at the optimum tube path associated with this p2p trajectory. Constraint (35) obligates that at $\Phi^*[k,\mathcal{E}]$ RISeUAV is located inside the sphere of the optimum waypoint k, which is also the starting point of $\Phi^*[k+1]$. Constraints (36) and (37) are the LoS link and SNR constraints, respectively.

To solve the problem in (32), the time interval $\mathcal{T}[k]$ associated with tube path $\Phi^*[k]$ is also divided into $\mathcal{E}$ equal time slots with time sampling interval δ, so that we have $\mathcal{T}[k] = \{\delta, 2\delta, \dots, \mathcal{E}\delta\}$. Since the RIS faces the ground, the channel performance can be independent of $\theta[k,\epsilon]$ (i.e., the heading of the UAV with respect to the x-axis), thanks to the intelligent phase-shift matrix and passive beamforming. Thus, $\theta[k,\epsilon]$ is not considered as an optimizing variable, but as a constraint to limit angular speed, that can be achieved based on the UAV positions at two consecutive slots (i.e., $\Phi^*[k,\epsilon-1]$ and $\Phi^*[k,\epsilon]$). Therefore, the cost function (32) can be written in (P1) as predictive finite receding horizon optimization for RISeUAV navigation while considering the channel performance (henceforth, we eliminate index k associated with the k^{th} p2p trajectory, for the sake of simplicity).

$$\text{(P1):} \min_{\mathbb{u}[\epsilon]} \quad \sum_{\epsilon=1}^{\mathcal{E}} (\|(p^{MT}[\epsilon] - p[\epsilon])\|_2 \|(p[\epsilon] - p_n^{BS})\|_2), \tag{38}$$

$$s.t. \quad p[\epsilon+1] = \mathbb{A}p[\epsilon] + \mathbb{B}\mathbb{u}[\epsilon+1] + \mathbb{D}, \tag{39}$$

$$v^* \le v[\epsilon] = \left\|\left[v_x(t), v_y(t)\right]^T\right\|_2 < V_{max}, \forall\, \epsilon \in \mathbb{E}, \tag{40}$$

$$|u[\epsilon]| < U_{max}, \forall\, \epsilon \in \mathbb{E}, \tag{41}$$

$$\left|\tan^{-1}\left(\frac{v_y[\epsilon]}{v_x[\epsilon]}\right) - \theta[\epsilon-1]\right| < \delta\frac{W_{max}}{v[\epsilon]}, \forall\, \epsilon \in \mathbb{E}, \tag{42}$$

$$p[\epsilon] \in \Phi^*, \forall\, \epsilon \in \mathbb{E}, \tag{43}$$

$$p[\mathcal{E}] \in \mathcal{S}^*[k], \tag{44}$$

$$\left(\vec{\Delta}_n^{BSRU}[\epsilon] \cup \vec{\Delta}^{RUMT}[\epsilon]\right) \cap\ p_\Omega^{3D} = \emptyset, \forall\, \epsilon \in \mathbb{E}, \tag{45}$$

$$\|(p^{MT}[\epsilon] - p[\epsilon])\|_2 \|(p[\epsilon] - p_n^{BS})\|_2 < \Delta_{max}, \quad \forall\, \epsilon \in \mathbb{E}, \tag{46}$$

where $\mathbb{A} = I_{3\times 3}$, $\mathbb{B} = \delta I_{3\times 3}$, $\mathbb{u}[\epsilon] = [v_x[\epsilon],\ v_y[\epsilon],\ u[\epsilon]]^T$ including the optimizing variables, and $\mathbb{D} = [0\ \ 0\ \ -u_0]^T$, which are developed by discretizing the kinematic equation of motion in (2); $p[0] = Q[k-1, q_{k-1}^*]$, i.e., the initial RISeUAV position is given by the last optimal position at the end of the previous p2p trajectory.

We model the receding potential trajectory of the RISeUAV using model predictive control in (39), where (40)-(41) impose speed constraints. Constraint (42) limits the RISeUAV heading rate and satisfies the nonholonomic constraint. We do not bound the vertical speed to the vertical speed given by stage 1 because the RISeUAV may keep the initial altitude, or even reduce the altitude at the first time slots to increase the channel gain. The SNR constraint in (37) is modeled by (46), where Δ_{max} denotes the maximum value that ensures that the minimum SNR is achieved. However, the optimization problem (P1) is non-convex with non-convex constraints in (42)-(46). With a relatively low altitude (z), the product of two 2-norm approaches zero when the RISeUAV gets close to a BS or the MT. At a relatively high altitude, the problem is convex. We first consider the RISeUAV−MT distance to be minimized because the RISeUAV p2p trajectory is limited to the secured tube path which preserves the validity of the BS-RISeUAV link and channel gain. Also, this is aligned with the problem objective, i.e., minimizing the channel gain and ensuring that RISeUAV

can track the MT movement in time. Further, considering that the minimum SNR constraint is satisfied at both ends of the tube path and the optimization problem is to minimize the link distance, we can relax the minimum SNR constraint in (46). Therefore, we focus on solving (P2) as:

$$\text{(P2):}\quad \min_{\mathfrak{U}} \left\| \mathfrak{B}\mathfrak{U} - \left(p_{\mathcal{E}}^{MT} - (\boldsymbol{\mathcal{A}}p[0] + \mathfrak{D}\boldsymbol{\Lambda})\right)\right\|_2 \tag{47}$$

$$s.t.\quad p[\epsilon] = \boldsymbol{\mathcal{A}}_\epsilon p[0] + \mathfrak{B}_\epsilon \mathfrak{U}_\epsilon + \mathfrak{D}_\epsilon \boldsymbol{I}_{\mathbf{1\times 3\epsilon}}; \tag{48}$$

$$v^* \le \left\| [v_x(t), v_y(t)]^T \right\|_2 < V_{max}, \forall\, \epsilon \in \mathbb{E}, \tag{49}$$

$$|u[\epsilon]| < U_{max}, \forall\, \epsilon \in \mathbb{E}, \tag{50}$$

$$\begin{matrix} v_x[\epsilon] - v_x[\epsilon-1]\left(1 - \frac{1}{V_{max}}\right) > 0, \\ \left(v_y[\epsilon] - v_y[\epsilon-1]\left(1 - \frac{1}{V_{max}}\right) > 0, \right. \end{matrix} \quad \forall\, \epsilon \in \mathbb{E}, \tag{51}$$

$$p_{min}^{\Phi^*}[\epsilon] \le p[\epsilon] \le p_{max}^{\Phi^*}[\epsilon], \forall\, \epsilon \in \mathbb{E}, \tag{52}$$

$$z[\epsilon] \ge z_n^{BS} + z, \tag{53}$$

$$p[\mathcal{E}] = Q[k, q_k^*], \tag{54}$$

$$\left(\vec{\Delta}_n^{BSRU}[\epsilon] \cup \vec{\Delta}^{RUMT}[\epsilon]\right) \cap\ p_\Omega^{3D} = \emptyset, \forall\, \epsilon \in \mathbb{E}, \tag{55}$$

where $\mathfrak{U} = [\mathbb{u}[1]\quad \mathbb{u}[2]\quad \mathbb{u}[3]\quad \cdots\quad \mathbb{u}[\mathcal{E}]]^T$;

$\mathfrak{U}_\epsilon = [\mathbb{u}[1]\quad \mathbb{u}[2]\quad \mathbb{u}[3]\quad \cdots\quad \mathbb{u}[\epsilon]]^T$;

$p_{\mathcal{E}}^{MT} = [P^{MT}[1]\quad P^{MT}[2]\quad P^{MT}[3]\quad \cdots\quad P^{MT}[\epsilon]]^T$;

$\boldsymbol{\mathcal{A}}_\epsilon = \mathbb{A}^\epsilon$; $\boldsymbol{\mathcal{A}} = [\mathbb{A}\quad \mathbb{A}^2\quad \mathbb{A}^3\quad \cdots\quad \mathbb{A}^\epsilon]^T$;

$\mathfrak{B}_\epsilon = [\mathbb{A}^{\epsilon-1}\mathbb{B}\quad \mathbb{A}^{\epsilon-2}\mathbb{B}\quad \ldots\quad \mathbb{A}\mathbb{B}\quad \mathbb{B}]$;

$\mathfrak{D}_\epsilon = [\mathbb{A}^{\epsilon-1}\mathbb{D}\quad \mathbb{A}^{\epsilon-2}\mathbb{D}\quad \ldots\quad \mathbb{A}\mathbb{D}\quad \mathbb{D}]$;

$$\mathfrak{B} = \begin{bmatrix} \mathbb{B} & 0 & \ldots & 0 & 0 \\ \mathbb{A}\mathbb{B} & \mathbb{B} & \ldots & 0 & 0 \\ \mathbb{A}^2\mathbb{B} & \mathbb{A}\mathbb{B} & \ddots & 0 & 0 \\ \vdots & \vdots & \ddots & \mathbb{B} & 0 \\ \mathbb{A}^{\mathcal{E}-1}\mathbb{B} & \mathbb{A}^{\mathcal{E}-2}\mathbb{B} & \ldots & \mathbb{A}\mathbb{B} & \mathbb{B} \end{bmatrix};$$

$$\mathfrak{D} = \begin{bmatrix} \mathbb{D} & 0 & \ldots & 0 & 0 \\ \mathbb{A}\mathbb{D} & \mathbb{D} & \ldots & 0 & 0 \\ \mathbb{A}^2\mathbb{D} & \mathbb{A}\mathbb{D} & \ddots & 0 & 0 \\ \vdots & \vdots & \ddots & \mathbb{D} & 0 \\ \mathbb{A}^{\mathcal{E}-1}\mathbb{D} & \mathbb{A}^{\mathcal{E}-2}\mathbb{D} & \ldots & \mathbb{A}\mathbb{D} & \mathbb{D} \end{bmatrix};$$

$\boldsymbol{\Lambda} = (\alpha_{ij}) \in \mathbb{R}^{3\mathcal{E}\times 3\mathcal{E}}$ with $(\alpha_{ij}) = 1\ \ if\ \ i \ge j\ \ or\ \ 0$ otherwise. $p_{min}^{\Phi^*}[\epsilon]$ and $p_{max}^{\Phi^*}[\epsilon]$ are the 3D Cartesian coordinates achieved based on the cylinder that models the tube path, as shown in Fig. 2. To deal with the nonconvexity of constraints (42) and (43), and for modeling the cylinder of tube path and cone region that satisfies speed constraints, we apply piecewise linearization as described in the sequel. From two given positions at both ends of p2p trajectory k (i.e., $p[0] = Q[k-1, q_{k-1}^*]$ and $p[\mathcal{E}] = Q[k, q_k^*]$), we can get the azimuth and elevation angles of the cylinder corresponding to tube path k:

$$\varphi_k = \cos^{-1}\left(\frac{x_k^* - x_{k-1}^*}{\|[(x_k^* - x_{k-1}^*), (y_k^* - y_{k-1}^*)]^T\|_2}\right); \tag{56}$$

$$\zeta_k = \tan^{-1}\left(\frac{z_k^* - z_{k-1}^*}{\|[(x_k^* - x_{k-1}^*), (y_k^* - y_{k-1}^*)]^T\|_2}\right). \tag{57}$$

Then we discretize the cylinder axis into $\mathcal{E}$ slots and calculate the discretized boundaries of the cylinder for slot ϵ as:

$$p_{max,min}^{\Phi^*}[\epsilon] = p[0] + \partial\left((\zeta_k), (\varphi_k)\right)\left(\epsilon\frac{\|p[\mathcal{E}] - p[0]\|_2}{\mathcal{E}}\right) \pm r I_{3\times 1}, \tag{58}$$

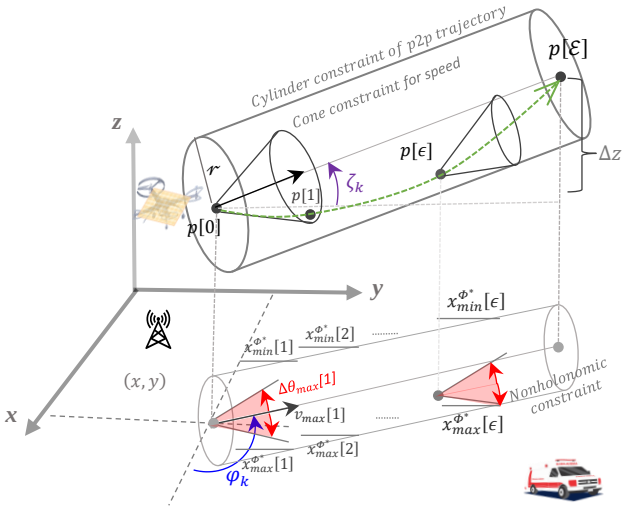

Fig. 2. RISoUAV navigation through the cylinder of the p2p tube path.

where $\partial\left((\zeta_k), (\varphi)\right)$ denotes the normalized vector of tube path k and is given as

$$\partial\left((\zeta_k), (\varphi_k)\right) = \begin{bmatrix} \cos(\zeta_k)\cos(\varphi_k) \\ \cos(\zeta_k)\sin(\varphi_k) \\ \sin(\zeta_k) \end{bmatrix}^T.$$

Constraint (52) is developed due to the fact that:

$$\left(\tan^{-1}\left(\frac{v_y}{v_x}\right)\right)' = \frac{{v_x}^2}{{v_x}^2 + {v_y}^2} \approx \frac{v_x}{v}. \tag{59}$$

Since the largest possible value for v is V_{max}, we constrain the lower bound of $v_x[\epsilon]$, by limiting the difference between consecutive slots by $v_x[\epsilon] - v_x[\epsilon-1] > \frac{v_x[\epsilon-1]}{V_{max}}$; and we consider the same constraints for the lower bound of $v_y[\epsilon]$, which constrains the upper bound of $v_x[\epsilon]$ based on (49), and vice versa. For the first slot, we put $v_x[\epsilon-1] = v^*\cos(\varphi_k)$ and $v_y[\epsilon-1] = v^*\sin(\varphi_k)$, where v^* is the optimal speed of p2p trajectory k given by stage 1. Constraint (43) can be linearly obtained by (48) and (52) with the aid of (58). Therefore, constraints (49)-(51) model the cone speed constraint; constraint (52) models the cylinder of the p2p trajectory; constraint (53) ensures that the altitude of the RISeUAV is comparatively higher than the altitude of the BS to secure the LoS link. Here, we assume that the p2p tube path is free of physical obstacles achieved in stage 1.

Nevertheless, the boundaries of the cylinder might be occupied by some buildings that can be identified based on the occupancy map and can be modeled as constraints in P2 that must be avoided. This can be implemented by checking the validity of the cylinder constraints in (52) with the occupancy map and replacing them with valid constraints, which obviously shrink the tube path. However, still, real-time modeling of the LoS link in (55) is a problem. We change (44) to (54) because the LoS link of $Q[k, q_k^*]$ has been secured in stage 1.

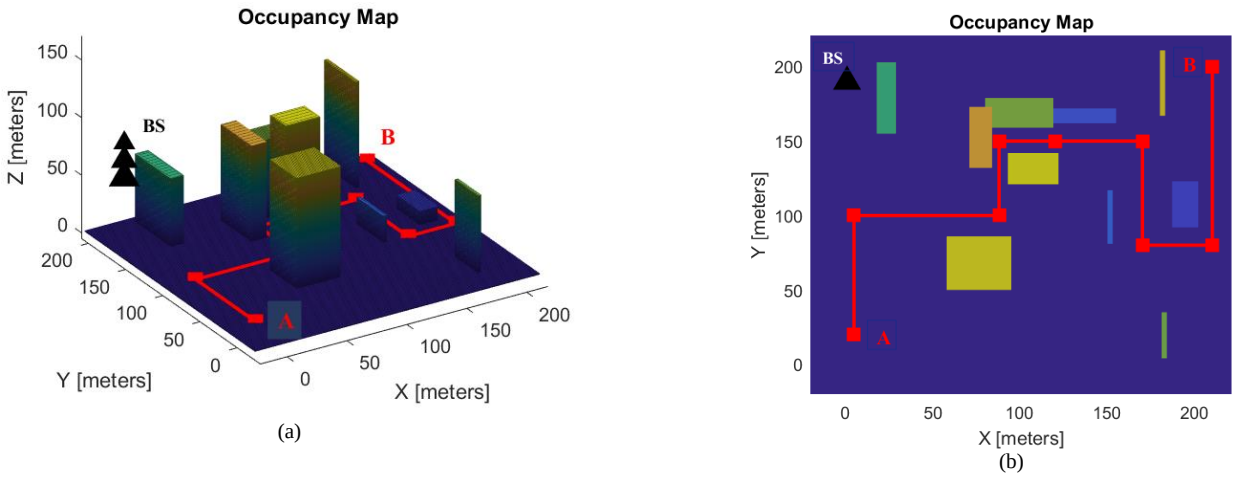

(a) (b)

Fig. 3. The 3D map of the simulated dense urban area: (a) the 3D occupancy map and MT route from point A to point B; (b) the MT route in the XY plane. The MT map route is divided into 8 slots by 9 waypoints: $\Re[k]|\ \forall\ k = 1, \ldots, 9$, which are shown by red squares.

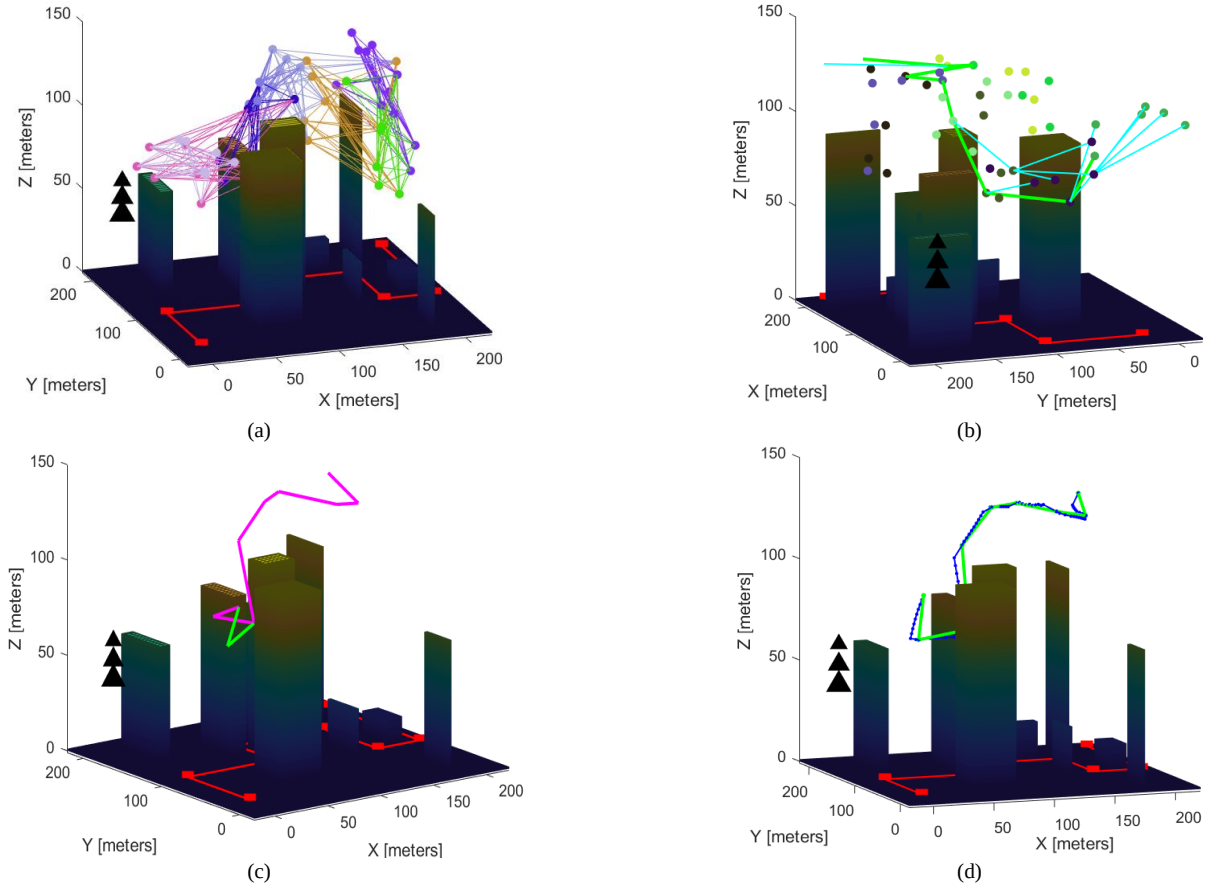

(a) (b)

(c) (d)

Fig. 4. Simulation results for the dense urban scenario: (a) stage 1, all possible p2p paths through random options; (b) $\aleph$ prospective trajectories with valid speeds/accelerations (shown by light blue lines) and selected trajectory with minimum energy consumption (shown by light green lines); (c) trajectory with minimum energy consumption (shown by light green) vs. trajectory found by DP (shown by pink); (d) optimum trajectory through the second stage for RISeUAV guidance (shown by blue lines).

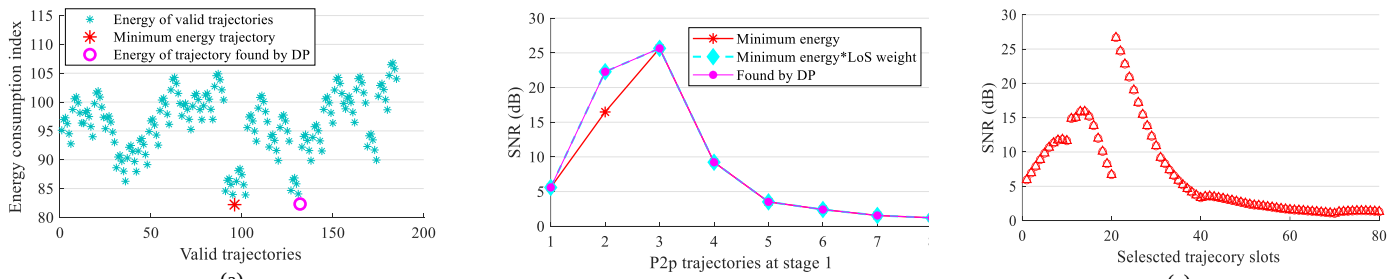

(a) (b) (c)

Fig. 5. Numerical result for the simulated scenario: (a) Energy consumption indicator for valid trajectories; (b) SNR at p2p waypoints of the selected trajectories; (c) SNR for the trajectory slots of the optimum trajectory.

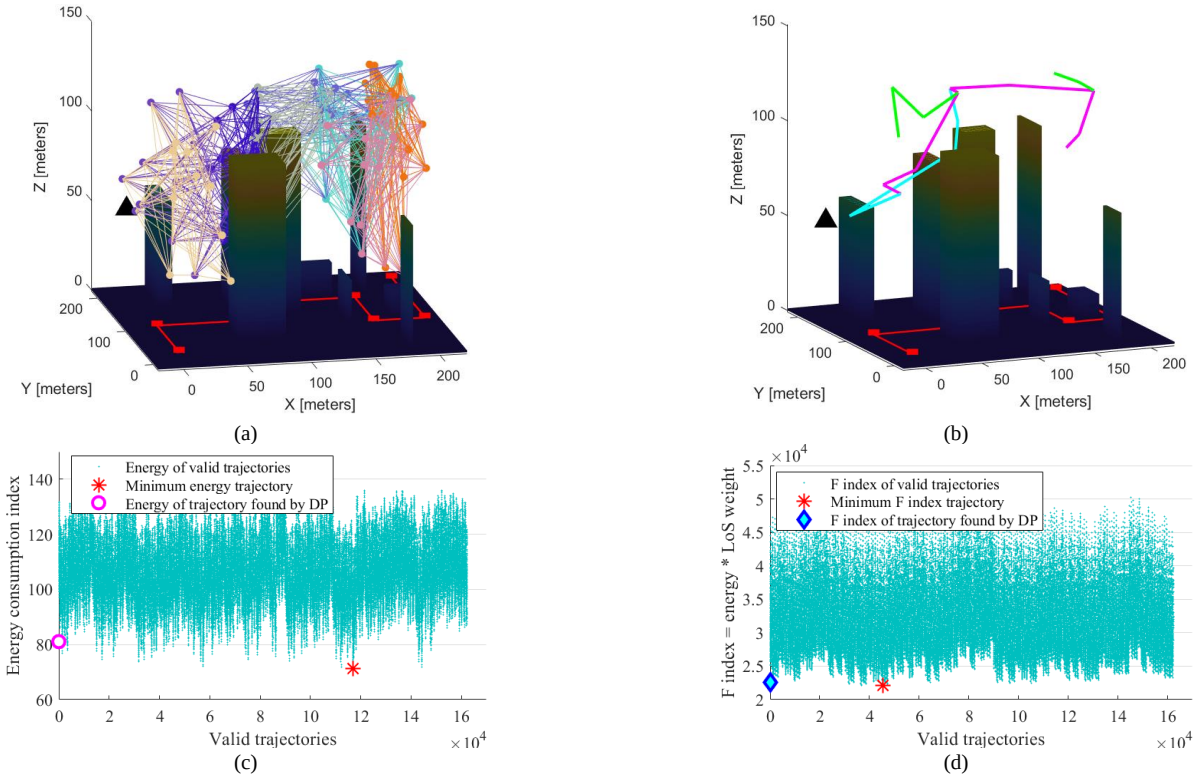

Fig. 6. Simulation results for assessing the DP performance in stage 1: (a) all possible p2p paths with 10 random options for each p2p path; (b) trajectory with minimum energy consumption (shown by light green) vs. trajectory found by DP (shown by pink), and trajectory with minimum F index = energy × LoS weight ((shown by light blue); (c) Energy consumption indicator for valid trajectories; (d) F index for valid trajectories.

Then, (55) can be embedded in (52), while the areas of the cylinder where the LoS link is unavailable can be regarded as obstacles. The validity of the LoS link at cylinder boundaries corresponding to each slot can be verified by interpolating the BS−RISeUAV −MT link for cylinder boundaries in (58) and checking the validity of intermediate points with the occupancy map. Nevertheless, efficient modeling of the LoS link in (55) in the context of convex optimization is part of our future work. Finally, in special cases, if the map route of the MT corresponding to the p2p trajectory k is aligned with the vector $\vec{\Delta}_n^{BSMT}[k]$, the solution to (P2) would be close to the solution to (P1).

If the map route of the MT corresponding to the p2p trajectory k is perpendicular to the vector $\vec{\Delta}_n^{BSMT}[k]$, (P3) can be solved for the $\vec{\Delta}_n^{BSRU}[k,\epsilon]$ link as

$$\text{(P3):}\ \min_{\mathfrak{U}}\ \left\|\mathfrak{B}\mathfrak{U}-\left(p_n^{BS}-\left(\mathcal{A}p[0]+\mathfrak{D}\mathbf{\Lambda}\right)\right)\right\|_2 \qquad (60)$$
$$s.t.\quad (48)-(55);$$

and the optimal solution would be the average of solutions to (P2) and (P3).

C. Time Complexity of the Proposed DP-MPC Method

The time complexity of the trajectory design with the proposed DP-MPC method is approximated by

$$T = T_{DP} + T_{MPC} = \mathcal{O}(K) + \left(\mathcal{O}(K \times P2) + \mathcal{O}(K \times P3)\right) \approx \mathcal{O}\left(K\left(1 + 2\log\left(\frac{1}{\varepsilon_0}\right)\right)\right);$$

where ε_0 denotes the accuracy of the interior-point method. The time complexity is significantly lower than that of the RRT method which is $\left(\mathcal{O}(Q^{K+1})\right)$.

IV. Simulation Results

The RISeUAV navigation in a dense urban area is simulated on the Matlab platform to evaluate the effectiveness of the proposed method. The 3D occupancy map of the simulated scenario is presented in Fig. 3. The MT is moving from point A to point B through the MT route shown by the red tracks.

The occupancy map is validated through the Matlab UAV toolbox (unoccupied map points are considered valid states and occupied and unknown map locations are interpreted as invalid states). The system parameters are $P_{BS} = 30$ dBm, $\sigma^2 = -80$ dBm, $\rho = 10$ dBm, $\gamma = 2$, $\lambda = 10^{-2}$ m, and $d = \frac{1}{2}\lambda$.

To find an energy-efficient and LoS-secured tube path for the RISeUAV to follow the MT, the A-B route is divided into 8 slots by choosing 9 waypoints including the starting point and the endpoint of the MT route and crosspoints of streets and the middle of the long streets in dense areas. The MT travel time (the time indicator), based on which the RISeUAV navigation and speed/acceleration limits are determined, is selected as

$\mathcal{T}[k] = \{8 \quad 8.3 \quad 5.2 \quad 4.1 \quad 4 \quad 7 \quad 4 \quad 12\}$ seconds.

For each waypoint $\Re[k]|\ \forall\, k \in \{0,\dots,8\}$, 6 random options $\mathcal{Q}[k,q_k]\ \forall\, q_k = 1,\dots,6$ are allocated, see Fig. 4(a), that satisfy the following constraints; $35\ m \le z \le 130\ m$, $r = 15\ m$, and maximum horizontal distance from waypoint k (i.e., $\Re[k]$) for allocated random options is 50 m.

Also, the allocated random options must satisfy the

BS−RIS−MT LoS and SNR constraints and there must be a valid path between $Q[k-1, q_{k-1}]$ and $Q[k, q_k]$. Increasing (decreasing) the number of allocated random options for each waypoint (the sphere radius r) increases the chance of getting a valid optimal tube path but increases the computational burden.

The number of paths through the allocated random options is very large (i.e., 6^9). Nevertheless, after applying the RISeUAV speed/acceleration constraints ($V_{max} = 12\frac{m}{s}, U_{max} = 8\frac{m}{s}, W_{max} = \pi/6\ \frac{rad}{slot}$), the number of valid prospective paths reduces to approximately 180 trajectories, see Fig. 4(b). Then, the trajectory with the minimum energy consumption is selected by which the energy-efficient and LoS/SNR-secured tube path for the second stage is achieved, see Fig. 4(c). At the second stage, using convex optimization to solve (P2) and (P3), the final optimal trajectory is obtained, see Fig. 4(d). In this regard, we use Optimization Toolbox in Matlab (*fmincon* syntax). The number of assigned slots for each p2p path is selected to be 10 for the second stage (a total of 80 slots for the whole RISeUAV trajectory). The energy index and achieved SNRs for trajectory slots ($SNR_{min} = 1$) are shown in Fig. 5.

The performance of DP in finding the optimum trajectory among all valid trajectories is evaluated, revealing promising performance. With a laptop computer (Processor Intel(R) Core(TM) i7-8665U CPU @ 1.90GHz, RAM 32.0 GB), it took 4.9 seconds to find the trajectory with minimum energy index = 82.2182, whereas DP found a trajectory with an energy index = 82.3221 in 0.001 seconds based on the Matlab *tic-toc* function, see Fig. 5(a).

To further analyze the global optimality of the solution, we simulate a scenario with ten random options for p2p paths, as illustrated in Fig. 6. The number of all paths increases to 10^9 with approximately 160,000 valid trajectories; see Fig. 6(a). It took 15.5 seconds to find the optimal trajectory with the minimum energy index of 77.7489, whereas DP found a trajectory with an energy index of 84.45 in 0.0045 second recorded by the Matlab tic-toc function; see Figs. 6(b) and (c). The interesting point is that after replacing the energy index with the F_index = energy × LoS weight in (25), DP finds the optimal trajectory with the minimum F_index, see Fig. 6(d). Overall, after averaging the results of several runs of stage 1 and comparing DP results with optimal results given by nonpolynomial exhaustive search, DP achieves approximately 90% of the global optimum with less than 1% of the computational burden.

V. Discussion

Based on the simulation results, the proposed method successfully discovers an energy-efficient and LoS-secured path for RISoUAV navigation to maintain LoS wireless communication link for the MT. The second stage determines the final trajectory by considering the energy index and channel performance as objectives while satisfying the UAV motion and nonholonomic constraints. The performance of the second stage strongly depends on the first stage as the second stage is restricted by the factors determined by the first stage such as radius r and speed constraints.

However, designing the system parameters (for modeling the problem and developing a solution) depends on the UAV and environmental characteristics in the first stage. For instance, in terms of the computational burden, selecting the number of planning slots and sphere radius r depends on the performance of the computational burden. From the UAV flight perspective, several factors, such as the UAV maneuvers (speed/acceleration) limits, the maximum flight altitude for allocating potential options for each waypoint (at stage 1), the height of buildings, density of the urban area, etc., have impact on the performance and convergence of the method. From the channel performance point of view, achieving an acceptable SNR (while satisfying the LoS and flight constraints) depends on the BSs allocations, power rating of the incident signals, the number of RIS elements, the flight altitude, etc. In this light, we considered one BS to simulate a worst-case scenario in the simulated scenario to see if the proposed method can successfully find an appropriate navigation path for the RISoUAV to satisfy problem constraints. It is observed that the achieved SNR at the last slots (where the MT is far from the BS and the UAV has to fly at a higher altitude to secure the LoS) declines. Considering other BSs of terrestrial 5G WCNs, increasing the power rating of the communication signal, and adopting larger RISs with more elements can be helpful but cost more. Thus, securing the convergence of the method in the first stage to a valid solution demands a compromise between the level of reliability/security requirements and costs that depends on environmental characteristics.

The practical limitations of the RIS phase shift following the UAV maneuver and imperfect CSI are not considered in this work and will be our future work. Also, uncertainty in MT motion and sudden route changes due to traffic and other vehicles are issues that can be considered to extend the work. However, the RIS can be embodied as a smooth, reflective, metallic surface in the case of quasi-optical mmWave signals, or a mirror in the case of visible light communications. A UAV can locate the vehicles using computer vision-based video odometry and reconfigure its RIS when the BS and intelligent vehicle have unobstructed LoS to the UAV. Further, a potential research topic is the UAV navigation design when the 3D map is unavailable, and UAV flight relies on UAV sensors. For example, vision-based navigation based on deep (reinforcement) learning methods is suggested.

VI. Conclusion

The autonomous navigation of a UAV equipped with an RIS was designed to secure the LoS communication link for a mobile vehicle (an emergency ambulance) in 5G-6G WCNs. To tackle the computational burden of achieving an optimal energy-efficient and LoS-secured path while capturing the UAV flight constraints and BS−RIS−MT channel performance, a two-stage method was proposed. Stage 1 is an offline process (while the RISeUAV is preparing for the trip) to find an LoS-secured tube path with minimum energy consumption that satisfies the RISeUAV motion constraints. Stage 1 was modeled as a traveling salesman problem using a semi-RRT method and dynamic programming was adopted to make the solution computationally tractable. Stage 2 can be executed in real-time during the flight for the next p2p trajectory as a finite receding horizon aiming at maximizing the channel gain and thus the achievable rate. To this end, we

modeled the problem as convex non-linear quadratic programming with a mix of non-linear quadratic and linear constraints, which can be solved in real-time utilizing existing solvers such as the interior-point method.

REFERENCES

[1] Q. Quan, R. Fu, M. Li, D. Wei, Y. Gao and K. -Y. Cai, "Practical Distributed Control for VTOL UAVs to Pass a Virtual Tube," in *IEEE Transactions on Intelligent Vehicles*, vol. 7, no. 2, pp. 342-353, June 2022.

[2] E. N. Barmpounakis, E. I. Vlahogianni and J. C. Golias, "Identifying Predictable Patterns in the Unconventional Overtaking Decisions of PTW for Cooperative ITS," in *IEEE Transactions on Intelligent Vehicles*, vol. 3, no. 1, pp. 102-111, March 2018.

[3] R. W. Beard, T. W. McLain, M. A. Goodrich and E. P. Anderson, "Coordinated target assignment and intercept for unmanned air vehicles," in *IEEE Trans. on Rob. and Auto.*, vol. 18, no. 6, pp. 911-922, Dec. 2002.

[4] W. Meng, Z. He, R. Su, P. K. Yadav, R. Teo and L. Xie, "Decentralized Multi-UAV Flight Autonomy for Moving Convoys Search and Track," in *IEEE Trans. on Cont. Syst. Tech.*, vol. 25, no. 4, pp. 1480-1487, 2017.

[5] Y. -J. Chen, D. -K. Chang and C. Zhang, "Autonomous Tracking Using a Swarm of UAVs: A Constrained Multi-Agent Reinforcement Learning Approach," in *IEEE Trans. on Vehicular Tech.*, vol. 69, no. 11, pp. 13702-13717, Nov. 2020.

[6] D. H. Choi, S. H. Kim and D. K. Sung, "Energy-efficient maneuvering and communication of a single UAV-based relay," in *IEEE Transactions on Aerospace and Electronic Systems*, vol. 50, no. 3, pp. 2320-2327, July 2014.

[7] F. Zhou, X. Li, M. Alazab, R. H. Jhaveri and K. Guo, "Secrecy Performance for RIS-based Integrated Satellite Vehicle Networks with A UAV Relay and MRC Eavesdropping," in *IEEE Transactions on Intelligent Vehicles*, doi: 10.1109/TIV.2022.3225466.

[8] R. Liu *et al*., "DRL-UTPS: DRL-based Trajectory Planning for Unmanned Aerial Vehicles for Data Collection in Dynamic IoT Network," in *IEEE Transactions on Intelligent Vehicles*, 2022, doi: 10.1109/TIV.2022.3213703.

[9] J. Lyu, Y. Zeng, R. Zhang and T. J. Lim, "Placement Optimization of UAV-Mounted Mobile Base Stations," in *IEEE Communications Letters*, vol. 21, no. 3, pp. 604-607, March 2017.

[10] Q. Wu, Y. Zeng and R. Zhang, "Joint Trajectory and Communication Design for Multi-UAV Enabled Wireless Networks," in *IEEE Transactions on Wireless Communications*, vol. 17, no. 3, pp. 2109-2121, March 2018.

[11] N. Souli, P. Kolios and G. Ellinas, "Online Relative Positioning of Autonomous Vehicles using Signals of Opportunity," in *IEEE Transactions on Intelligent Vehicles*, 2022.

[12] T. E. Bogale, X. Wang, and L. B. Le. "mmWave communication enabling techniques for 5G wireless systems: A link level perspective." In *MmWave Massive MIMO*, pp. 195-225. Academic Press, 2017.

[13] E. Basar, M. Di Renzo, J. De Rosny, M. Debbah, M. -S. Alouini and R. Zhang, "Wireless Communications Through Reconfigurable Intelligent Surfaces," in *IEEE Access*, vol. 7, pp. 116753-116773, 2019.

[14] M. A. ElMossallamy, H. Zhang, L. Song, K. G. Seddik, Z. Han and G. Y. Li, "Reconfigurable Intelligent Surfaces for Wireless Communications: Principles, Challenges, and Opportunities," in *IEEE Transactions on Cognitive Communications and Networking*, vol. 6, no. 3, pp. 990-1002, Sept. 2020.

[15] W. Tang *et al*., "Wireless Communications With Reconfigurable Intelligent Surface: Path Loss Modeling and Experimental Measurement," in *IEEE Trans. on Wireless Communications*, vol. 20, no. 1, pp. 421-439, Jan. 2021.

[16] Q. Wu and R. Zhang, "Intelligent reflecting surface-enhanced wireless network via joint active and passive beamforming," *IEEE Trans. Wireless Communications.*, vol. 18, no. 11, pp. 5394–5409, Nov. 2019.

[17] C. Huang, A. Zappone, G. C. Alexandropoulos, M. Debbah and C. Yuen, "Reconfigurable Intelligent Surfaces for Energy Efficiency in Wireless Communication," in *IEEE Transactions on Wireless Communications*, vol. 18, no. 8, pp. 4157-4170, Aug. 2019.

[18] A. Bansal, N. Agrawal and K. Singh, "Rate-Splitting Multiple Access for UAV-Based RIS-Enabled Interference-Limited Vehicular Communication System," in *IEEE Transactions on Intelligent Vehicles*, 2022.

[19] Y. Pan, K. Wang, C. Pan, H. Zhu and J. Wang, "UAV-Assisted and Intelligent Reflecting Surfaces-Supported Terahertz Communications," in *IEEE Wireless Communications Letters*, vol. 10, no. 6, pp. 1256-1260, June 2021.

[20] Y. Zeng, J. Xu and R. Zhang, "Energy Minimization for Wireless Communication With Rotary-Wing UAV," in *IEEE Transactions on Wireless Communications*, vol. 18, no. 4, pp. 2329-2345, April 2019.

[21] S. Li, B. Duo, M. D. Renzo, M. Tao and X. Yuan, "Robust Secure UAV Communications With the Aid of Reconfigurable Intelligent Surfaces," in *IEEE Transactions on Wireless Communications*, vol. 20, no. 10, pp. 6402-6417, Oct. 2021.

[22] S. Li, B. Duo, X. Yuan, Y. Liang and M. Di Renzo, "Reconfigurable Intelligent Surface Assisted UAV Communication: Joint Trajectory Design and Passive Beamforming," in *IEEE Wireless Communications Letters*, vol. 9, no. 5, pp. 716-720, May 2020.

[23] X. Liu, Y. Liu and Y. Chen, "Machine Learning Empowered Trajectory and Passive Beamforming Design in UAV-RIS Wireless Networks," in *IEEE Journal on Selected Areas in Communications*, 2021.

[24] S. Alfattani *et al*., "Aerial Platforms with Reconfigurable Smart Surfaces for 5G and Beyond," in *IEEE Communications Magazine*, vol. 59, no. 1, pp. 96-102, January 2021.

[25] Q. Zhang, W. Saad, and M. Bennis. "Reflections in the sky: Millimeter wave communication with UAV-carried intelligent reflectors." In *2019 IEEE Global Communications Conference (GLOBECOM)*, pp. 1-6. IEEE, 2019.

[26] J. Khalife and Z. M. Kassas, "Differential Framework for Submeter-Accurate Vehicular Navigation with Cellular Signals," in *IEEE Transactions on Intelligent Vehicles*, 2022, doi: 10.1109/TIV.2022.3187957.

[27] M. Hosseini, Y. Jiang, R. R. Berlin, L. Sha and H. Song, "Toward Physiology-Aware DASH: Bandwidth-Compliant Prioritized Clinical Multimedia Communication in Ambulances," in *IEEE Trans. on Multimedia*, vol. 19, no. 10, pp. 2307-2321, Oct. 2017.

[28] Y. Zhai *et al*., "5G-Network-Enabled Smart Ambulance: Architecture, Application, and Evaluation," in *IEEE Network*, vol. 35, no. 1, pp. 190-196, January/February 2021.

[29] J. Y. Dai et al., "Wireless Communications through a Simplified Architecture Based on Time-Domain Digital Coding Metasurface," Adv. Mater. Tech., vol. 4, no. 7, July 2019, p. 1970037.

[30] W. Yao *et al*., "Evolutionary Utility Prediction Matrix-Based Mission Planning for Unmanned Aerial Vehicles in Complex Urban Environments," in *IEEE Transactions on Intelligent Vehicles*, 2022, doi: 10.1109/TIV.2022.3192525.

[31] N. Souli, P. Kolios and G. Ellinas, "Online Relative Positioning of Autonomous Vehicles using Signals of Opportunity," in *IEEE Transactions on Intelligent Vehicles*, doi: 10.1109/TIV.2021.3124727.

[32] S. P. Bharati, Y. Wu, Y. Sui, C. Padgett and G. Wang, "Real-Time Obstacle Detection and Tracking for Sense-and-Avoid Mechanism in UAVs," in *IEEE Transactions on Intelligent Vehicles*, vol. 3, no. 2, pp. 185-197, June 2018.

[33] A. V. Savkin, H. Huang and W. Ni, "Securing UAV Communication in the Presence of Stationary or Mobile Eavesdroppers via Online 3D Trajectory Planning," in *IEEE Wireless Communications Letters*, vol. 9, no. 8, pp. 1211-1215, Aug. 2020.

[34] J. Qian, K. Chen, Q. Chen, Y. Yang, J. Zhang and S. Chen, "Robust Visual-Lidar Simultaneous Localization and Mapping System for UAV," in *IEEE Geoscience and Remote Sensing Letters*, vol. 19, pp. 1-5, 2022.

[35] S. Hu, Z. Wei, Y. Cai, C. Liu, D. W. K. Ng and J. Yuan, "Robust and Secure Sum-Rate Maximization for Multiuser MISO Downlink Systems With Self-Sustainable IRS," in *IEEE Transactions on Communications*, vol. 69, no. 10, pp. 7032-7049, Oct. 2021.

[36] H. Oh, S. Kim, H. -s. Shin and A. Tsourdos, "Coordinated standoff tracking of moving target groups using multiple UAVs," in *IEEE Transactions on Aerospace and Electronic Systems*, vol. 51, no. 2, pp. 1501-1514, April 2015.

[37] R. E. Bellman, *Dynamic Programming*. Princeton, NJ, USA: Princeton Univ. Press, 1957.

[38] S. Rathinam, R. Sengupta and S. Darbha, "A Resource Allocation Algorithm for Multivehicle Systems With Nonholonomic Constraints," in *IEEE Transactions on Automation Science and Engineering*, vol. 4, no. 1, pp. 98-104, Jan. 2007.